Sub-Pixel Edge Detection of Circular Holes via Adaptive Filtering and Improved Zernike Moments

Weitang Zhang * and Senlin Dong

Posted Date: 2 May 2026

doi: 10.20944/preprints202604.2228.v1

Keywords: machine vision; edge detection; canny operator; Zernike moment; sub-pixel

 doi:10.20944/preprints202604.2228.v1

Article

Sub-Pixel Edge Detection of Circular Holes via Adaptive Filtering and Improved Zernike Moments

Weitang Zhang * and Senlin Dong

School of Electronic Information and Automation, Hefei University, Hefei 230601, China, d17766092656@163.com

* Correspondence: zhangweitang@hfuu.edu.cn

Abstract

To meet the requirements of high accuracy in image edge localization and strong noise resistance for computer vision calibration and precise measurement, an improved Zernike moment subpixel high-precision measurement method for circular hole-like workpieces is proposed. Firstly, the Canny operator is used as a coarse edge detection algorithm, with the traditional Gaussian filter in the Canny operator replaced by an improved Laplacian edge-adaptive median filter. This approach demonstrates improved edge preservation compared to traditional and adaptive median filtering, especially under high-concentration noise. Then, a subpixel edge detection algorithm is applied to refine the edges, thus enhancing the edge localization accuracy. An improved Zernike moment subpixel detection algorithm is employed for precise edge point detection. The improved algorithm selects a Zernike moment parameter template with higher detection accuracy. Finally, the inner and outer diameters of the circular hole-like part are measured by fitting the profile using the least squares method. Experimental results on several different workpieces demonstrate that the proposed algorithm achieves higher accuracy than the traditional Zernike moment subpixel method, with an error reduction of 75.1%, meeting the precision requirements in modern industrial part manufacturing processes.

Keywords: machine vision; edge detection; canny operator; Zernike moment; sub-pixel

1. Introduction

The circular hole-shaped components are commonly used mechanical parts in industry and are widely applied in various mechanical structures. The geometric dimensions of the circular hole are an important criterion for determining whether such components are qualified. Therefore, the measurement of the circular hole is a key aspect of mechanical component inspection. Existing methods for measuring the diameter of circular holes mainly include contact measurement methods, such as internal micrometers and calipers, as well as non-contact measurement methods, such as tool microscopes, bore interferometers, and X-ray instruments. The contact measurement methods are easily influenced by subjective judgment and the measuring tools themselves, with low efficiency, poor resistance to interference, and potential damage to the component surface. Additionally, some non-contact measurement methods involve high equipment costs, and some still require manual operation during the measurement process, leading to low efficiency and an inability to meet the requirements for online detection in industrial automated production.

The machine vision-based measurement method, however, offers advantages such as non-contact, high precision, and intelligence, making it well-suited to meet industrial needs. It has several advantages over manual measurement in the dimension measurement process and has broad application prospects.

In image measurement technology, edge detection is a core technique in the visual measurement process of circular holes and directly impacts the accuracy of online hole detection. Classical pixel-level edge detection algorithms typically rely on differential operators [11], such as the Canny

 doi:10.20944/preprints202604.2228.v1

operator [1], Sobel operator [2], Laplace operator [3], etc. Although most traditional edge detection algorithms are effective for detecting edges with pixel-level accuracy and the extracted edges can meet the measurement precision requirements in certain scenarios, they still fail to meet the precision needs in more demanding situations. Therefore, to achieve higher measurement precision, it is necessary to further investigate sub-pixel accuracy based on pixel-level detection. Currently, moment methods have become a popular research topic in sub-pixel edge detection, including grayscale moments, Zernike orthogonal moments, Franklin orthogonal moments, and others, among which Zernike orthogonal moments are widely applied.

Building on this, reference [4] proposed the rotation-invariant Zernike orthogonal moment, which offers faster processing speed and higher accuracy compared to the previous methods.

Subsequently, Bin introduced the Fourier-Mellin moment to address the limitation of Zernike moments in detecting small objects [5].

Reference [6] replaced the original template with a 9×9 template, resulting in better edge detection performance. However, as the template size increases, the detection results become more sensitive to noise. With the growing demand for higher dimensional precision in modern industry, this paper proposes an improved Zernike moment-based sub-pixel high-precision measurement method for circular hole-type components, aiming to enhance the detection accuracy.

In recent years, significant progress has been made in sub-pixel edge detection and machine vision measurement. Li et al. [12] developed an adaptive Zernike moment method combined with genetic algorithm optimization, which dynamically adjusts moment parameters according to local image features, achieving improved robustness against noise. Chen et al. [13] proposed an improved Canny edge detection algorithm integrating an adaptive median filter, demonstrating superior performance in preserving edge details under high-density salt-and-pepper noise. Wang et al. [14] presented a high-precision machine vision measurement system for circular holes using sub-pixel edge localization, which achieved measurement errors below 0.02 mm in industrial settings. Furthermore, Zhang et al. [15] introduced a deep learning-assisted Zernike moment framework that learns optimal edge models from training data, significantly enhancing sub-pixel accuracy in complex backgrounds. Liu et al. [16] developed an edge-preserving adaptive filtering technique specifically for salt-and-pepper noise removal, which maintains structural integrity while effectively eliminating impulsive noise. These recent advances provide valuable insights that complement and inspire the improvements proposed in this work.

2. The Improved Canny Operator Is Used for Coarse Pixel-Level Edge Extraction

In the field of digital image processing, noise removal is a fundamental and important task. Salt-and-pepper noise is a common type of noise that can significantly affect image quality. However, Gaussian filters have certain limitations, especially when dealing with images containing nonlinear noise, such as salt-and-pepper noise. This type of noise is often not effectively suppressed by linear filters. When an image contains a large amount of noise, stronger smoothing is typically needed to reduce the noise's impact. However, excessive smoothing can lead to the blurring of image edges, resulting in the loss of important edge information.

Moreover, the window size of the Gaussian filter needs to be manually set, which adds complexity when processing different images. Different images may require different window sizes to achieve optimal results. Therefore, the Canny edge detection algorithm exhibits certain limitations when handling diverse image types, especially in terms of adaptability. To address this issue, this paper proposes a method that combines adaptive median filtering with Laplacian edge detection.

2.1. Edge Adaptive Median Filtering

The traditional Canny edge detection algorithm employs a Gaussian filter to perform image smoothing. However, this method may result in excessive smoothing of edges during the filtering process, leading to the significant loss of fine edge details in the image. Traditional adaptive median filtering is highly effective for removing salt-and-pepper noise, as such noise is typically distributed

 doi:10.20944/preprints202604.2228.v1

at extreme values, and taking the median helps to avoid these noise points. However, under conditions of high noise concentration, increasing the window size to capture more neighboring pixels may introduce additional neighboring pixels, causing the blurring of image details and edge information. Additionally, there may be instances where the filter cannot completely remove all noise points, leaving residual noise that degrades the overall image quality.

Therefore, this paper proposes an edge-adaptive median filtering method based on the Laplacian operator. To prevent noise points from being selected during the median calculation, the first layer of the adaptive median filtering process is modified. Specifically, based on the initial calculation of $A_1 = Z_{med} - Z_{min}$ and $A_2 = Z_{max} - Z_{med}$, the difference between the maximum gray value Z_{max} and the minimum gray value Z_{min} within the pixel neighborhood is compared with Z_{med}. When salt-and-pepper noise is present in the image, Z_{max} is 255 and Z_{min} is 0. If $Z_{max} - Z_{min} > Z_{med}$, this further indicates the presence of salt-and-pepper noise. Then, the original algorithm, which outputs the median Z_{med}, is improved by replacing the output with the average gray value Z_{avg} of the remaining pixels after excluding the extreme maximum and minimum gray values. Otherwise, the output is the gray value at the pixel coordinates $Z_{xy}(x, y)$. Finally, the Laplacian operator is used to detect edges and determine whether the pixel value needs to be updated. The specific implementation steps are as follows:

Step 1: Initialize the filter window size $S_{xy} = 3$, and calculate the values of Z_{max}、Z_{med}、Z_{min} and Z_{xy}.

Step 2: Compute $A_1 = Z_{med} - Z_{min}$, $A_2 = Z_{max} - Z_{med}$, and determine the difference between Z_{max} and Z_{min}. If $A_1 > 0$, $A_2 > 0$, and $Z_{max} - Z_{min} > Z_{med}$, proceed to Step 3; otherwise, increase the window size. Additionally, check if S_{xy} exceeds S_{max}; if so, output Z_{xy}, otherwise, return to Step 1.

Step 3: Compute $B_1 = Z_{xy} - Z_{min}$ and $B_2 = Z_{max} - Z_{xy}$. If $B_1 > 0$ and $B_2 > 0$, output Z_{xy}; otherwise, output the average gray value Z_{avg} of the remaining pixels after excluding the extreme maximum and minimum gray values.

Step 4: Edge preservation. For each pixel (i, j), if the binary edge mask value detected by the Laplacian operator is 1, indicating that the pixel lies within an edge region, replace the filtered pixel value with the original pixel value from the image. If the corresponding value in the edge mask is not 1, indicating the pixel is not in an edge region, retain the pixel value from the filtered image.

This improved filtering mechanism offers better preservation of edge structures compared to conventional methods, as validated by recent studies on edge-preserving filtering [16]. The incorporation of Laplacian edge detection ensures that high-frequency edge information is retained while noise is effectively suppressed, leading to more reliable subsequent processing.

2.2. Improved Gradient Amplitude and Direction

The gradient magnitude and direction in the Canny edge detection algorithm are critical components. This step is used in image processing to identify edges within the image by calculating the gradient magnitude and direction at each pixel.

To preserve more edge information and ensure continuity of edges, an improvement is made to the original Canny operator by adding additional gradient directions: 0°, 22.5°, 45°, 67.5°, 90°, 112.5°, 135°, 157.5°, 180°, 202.5°, 225°, 247.5°, 270°, 292.5°, 315°, and 337.5°. The improved gradient magnitude and direction information is shown in Figure 1. The gradient magnitude for each pixel is computed according to the equations (1)–(18), as detailed below:

$$G_y(x, y) = f(x, y-1) - f(x, y+1) \quad (1)$$

$$G_x(x, y) = f(x+1, y) - f(x-1, y) \quad (2)$$

$$G_{0°}(x, y) = f(x+2, y) - f(x-2, y) \quad (3)$$

$$G_{22.5°}(x, y) = f(x+2, y+1) - f(x-2, y-1) \quad (4)$$

$$G_{45°}(x, y) = f(x+2, y+2) - f(x-2, y-2) \quad (5)$$

$$G_{67.5°}(x, y) = f(x+1, y+2) - f(x-1, y-2) \quad (6)$$

$$G_{90°}(x, y) = f(x, y+2) - f(x, y-2) \quad (7)$$

 doi:10.20944/preprints202604.2228.v1

$$G_{112.5°}(x,y) = f(x-1,y+2) - f(x+1,y-2) \quad (8)$$
$$G_{135°}(x,y) = f(x-2,y+2) - f(x+2,y-2) \quad (9)$$
$$G_{157.5°}(x,y) = f(x-2,y+1) - f(x+2,y-1) \quad (10)$$
$$G_{180°}(x,y) = f(x-2,y) - f(x+2,y) \quad (11)$$
$$G_{202.5°}(x,y) = f(x-2,y-1) - f(x+2,y+1) \quad (12)$$
$$G_{225°}(x,y) = f(x-2,y-2) - f(x+2,y+2) \quad (13)$$
$$G_{247.5°}(x,y) = f(x-1,y-2) - f(x+1,y+2) \quad (14)$$
$$G_{270°}(x,y) = f(x,y-2) - f(x,y+2) \quad (15)$$
$$G_{292.5°}(x,y) = f(x+1,y-2) - f(x-1,y+2) \quad (16)$$
$$G_{315°}(x,y) = f(x+2,y-2) - f(x-2,y+2) \quad (17)$$
$$G_{337.5°}(x,y) = f(x+2,y-1) - f(x-2,y+1) \quad (18)$$

In the equations, G(x, y) represents the first-order partial derivative. The improved gradient magnitude and gradient direction are given by equations (19) and (20), respectively.

$$W(x,y) = [(G_{0°})^2 + (G_{22.5°})^2 + (G_{45°})^2 + (G_{67.5°})^2 + (G_{90°})^2 + (G_{112.5°})^2 + (G_{135°})^2 + (G_{157.5°})^2 + (G_{180°})^2 + (G_{202.5°})^2 + (G_{225°})^2 + (G_{247.5°})^2 + (G_{270°})^2 + (G_{292.5°})^2 + (G_{315°})^2 + (G_{337.5°})^2]^{\frac{1}{2}} \quad (19)$$

$$D(x,y) = \text{argmax}_{k\in(0°,22.5°,45°,\ldots 337.5°)} G_k(x,y) \quad (20)$$

i.e., the gradient direction is chosen as the orientation with the maximum gradient magnitude among all 16 directions.

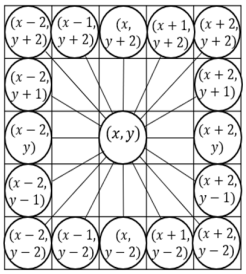

Figure 1. Gradient amplitude and direction information.

The traditional Canny edge detection algorithm primarily considers gradient magnitudes in the horizontal and vertical directions (i.e., 0° and 90°). This approach is sensitive to variations in image intensity and may overlook important edge information, especially for edges oriented at oblique angles, leading to misclassification of edges and broken edge contours. To enhance edge detection accuracy and reduce false positives, this paper proposes an improvement to the traditional algorithm by incorporating gradient magnitude calculations in 14 additional directions (22.5°, 45°, 67.5°, 112.5°, 135°, 157.5°, 202.5°, 247.5°, etc.), as shown in Figure 1. This modification helps minimize the loss of edge information and the misidentification of false edges, thereby improving the overall precision of edge recognition. Furthermore, the richer directional sampling enhances the continuity of detected edges and provides a more robust response to edges at various orientations, which is particularly beneficial for complex industrial images containing circular holes with varying curvature.

3. Traditional Zernike Moment Sub-Pixel Edge Detection Algorithm

3.1. Zernike Moment Principle

Current subpixel edge detection algorithms can be broadly categorized into three main types: the moment-based method [7], interpolation-based method [8], and fitting-based method [9]. Among

 doi:10.20944/preprints202604.2228.v1

them, the Zernike moment edge detection algorithm is invariant to image rotation and scaling, and exhibits robust noise resistance [10].

Zernike moments are defined in the set of complex valued functions with unit circle $x^2 + y^2 \leq 1$:

$$V_{nm}(x,y) = V_{nm}(\rho,\theta) = R_{nm}e^{im\theta} \quad (21)$$

In the formula: n, m are integers, $n \geq 0$, $n - |m|$ is an even number$|m| \leq n$, i is the imaginary unit.

The polynomial R_{nm} is expressed as follows:

$$R_{nm} = \sum_{s=0}^{\frac{(n-|m|)}{2}} \frac{(-1)^s (n-s)!\,\rho^{n-2s}}{s!\left(\frac{n+|m|}{2}-s\right)!\left(\frac{n-|m|}{2}-s\right)!} \quad (22)$$

In the unit circle $x^2 + y^2 = 1$, the Zernike moment for the discrete image f (x, y) is:

$$Z_{nm} = \frac{n+1}{\pi} \iint_{x^2+y^2\leq 1} f(x,y) V_{nm}^*(\rho,\theta)\,dx\,dy \quad (23)$$

In the formula: Z_{nm} denotes the n-th order m-th Zernike moment; $(n+1)/\pi$ is the normalization factor; * represents the complex conjugate; ϱ is the length of the vector from the origin to the point (x,y), and θ is the angle between this vector and the positive X-axis, measured counterclockwise; $V_{nm}^*(\rho,\theta)$ denotes the complex conjugate of the orthogonal complex polynomial function on the unit circle.

3.2. Zernike Moment Sub-Pixel Edge Detection Principle

To detect subpixel edges in an image using Zernike moments, an ideal grayscale step model is first established, where u represents the background grayscale value, v is the grayscale difference between the background and the foreground, with the foreground grayscale value being u+v, R denotes the ideal edge, and d is the perpendicular distance from the origin to the ideal edge R. This idealized model approximates local edge structures as a step function, which is a reasonable assumption for most industrial images. By utilizing the rotational invariance property of Zernike moments, an ideal rotationally invariant model is established. Specifically, the magnitudes of Zernike moments remain unchanged under image rotation, while only the phase angles are affected. As shown in Figure 2, the relationship between Z_{nm}' and Z_{nm} can be derived, enabling the extraction of edge parameters such as d and orientation α without explicitly searching along multiple directions. This property greatly simplifies the subpixel localization process.

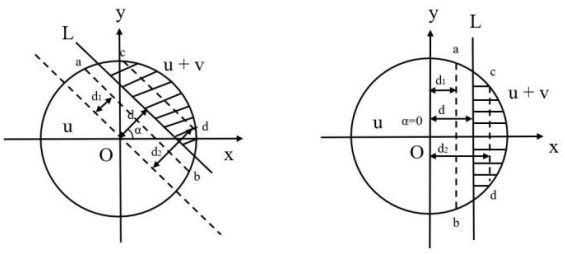

Figure 2. Ideal Edge Model.

It can be observed that the magnitudes of the Zernike moments remain the same before and after the transformation, with only the phase angle changing. Based on this relationship and the properties of Zernike moments, edge parameters can be determined by calculating three Zernike moments of different orders, such as Z_{00}, Z_{11}, and Z_{20}.Due to the rotational invariance property, it follows that:

Due to the symmetry of the image about the X-axis after rotating by an angle of φ, the imaginary part of Z_{11}' is 0, resulting in:

 doi:10.20944/preprints202604.2228.v1

$$\mathrm{Im}[Z_{11}^{'}] = \sin\varphi \mathrm{Re}[Z_{11}] - \cos\varphi \mathrm{Im}[Z_{11}] = 0$$

According to the ideal step model, the moments of each order after rotation are obtained as follows:

$$\begin{cases} Z_{00}^{'} = u\pi + \dfrac{v\pi}{2} - varcsin(d) - vd\sqrt{1-d^2} \\ Z_{11}^{'} = \dfrac{2v(1-d^2)^{\frac{3}{2}}}{3} \\ Z_{20}^{'} = \dfrac{2vd(1-d^2)^{\frac{3}{2}}}{3} \end{cases} \quad (24)$$

The ideal edge model parameters α, d, u, and v are obtained through equation (24):

$$\begin{cases} \alpha = \arctan\left(\dfrac{Im[Z_{11}]}{Re[Z_{11}]}\right) \\ d = \dfrac{Z_{20}}{Z_{11}^{'}} \\ v = \dfrac{3Z_{11}^{'}}{2(1-d^2)^{\frac{3}{2}}} \\ u = \dfrac{Z_{00} - \frac{v\pi}{2} + varcsin(d) + vd\sqrt{1-d^2}}{\pi} \end{cases} \quad (25)$$

When the unit circle is sampled using an N × N template in discrete situations, The calculation formula for Zernike moment sub-pixel coordinates is:

$$\begin{bmatrix} x^{'} \\ y^{'} \end{bmatrix} = \begin{bmatrix} x \\ y \end{bmatrix} + \frac{N}{2} d \begin{bmatrix} cos\alpha \\ sin\alpha \end{bmatrix} \quad (26)$$

The coordinates (x, y) represent the center of the unit circle, and $\alpha \backslash \mathrm{alpha} \alpha$ denotes the actual angle between the edge and the x-axis, which is calculated using (x, y) as the center of the convolution window.

4. Improved Zernike Moment Sub-Pixel Edge Detection Algorithm

4.1. Selection of Zernike Template Coefficients

In the subpixel detection process, selecting an appropriate Zernike template size is crucial for accuracy. Considering the requirements of this study, a 7×7 Zernike moment parameter template was chosen, striking a balance between detection accuracy and computational efficiency. The implementation of the optimization algorithm includes parallel processing and improvements in algorithm efficiency to ensure optimal performance.

4.2. Improvement of Edge Judgment Conditions in Zernike Moment Algorithm

The improved algorithm extends the Z_{00}, Z_{11}, andZ_{20} coefficients in the Ghosal algorithm to include Z_{31} and Z_{40} coefficient templates. Additionally, new edge determination conditions, $v \geq v_t$ and $d \geq d_t$, as well as $|d_2 - d_1| \leq d_t$, are introduced, replacing the traditional edge conditions $v \geq v_t$ and $d \leq d_t$. Here, d_t and v_t are threshold values determined by the average of the d and v matrices. The specific algorithm is as follows:

$$Z_{11}^{'} = \frac{2v(1-d^2)^{\frac{3}{2}}}{3} \quad (27)$$

$$Z_{20}^{'} = \frac{2vd(1-d^2)^{\frac{3}{2}}}{3} \quad (28)$$

$$Z_{31}^{'} = \frac{4vd^2(1-d^2)^{\frac{3}{2}}}{5} - \frac{2v(1-d^2)^{\frac{3}{2}}}{15} \quad (29)$$

 doi:10.20944/preprints202604.2228.v1

$$Z'_{40} = \frac{16vd^3(1-d^2)^{\frac{3}{2}}}{15} - \frac{2vd(1-d^2)^{\frac{3}{2}}}{5} \quad (30)$$

By solving equations (28) and (30):

$$d_1 = \sqrt{\frac{5Z'_{40} + 3Z'_{20}}{8Z'_{20}}} \quad (31)$$

By solving equations (27) and (29):

$$d_2 = \sqrt{\frac{5Z'_{31} + Z'_{11}}{6Z'_{11}}} \quad (32)$$

$$d = \frac{d_1 + d_2}{2} \quad (33)$$

5. Verification Results and Analysis

The experimental program in this paper is written in C++ and runs in the Visual Studio 2022 environment, utilizing OpenCV version 4.8.0. The hardware configuration consists of an i5-8250U processor with 8 GB of RAM. To validate and evaluate the effectiveness of the proposed algorithm, high-precision test images captured by an industrial CCD camera (1280 × 960 resolution) were selected for extensive experiments. These images include circular hole workpieces of different sizes and materials, captured under varying illumination conditions to ensure the comprehensiveness of the evaluation. Due to space limitations, four representative experimental images—covering different noise levels, edge complexities, and workpiece specifications—are presented and discussed here, which sufficiently demonstrate the performance of the proposed algorithm in terms of edge detection accuracy, noise robustness, and sub-pixel localization precision.

5.1. Filter Experiment Results

To quantitatively evaluate denoising performance, salt-and-pepper noise (1%-5.5%) was added to images. The proposed edge-adaptive median filter was compared against standard and adaptive median filters using PSNR and MSE metrics, as visual comparison proved inconclusive due to the subtle perceptual differences between the filtered outputs. PSNR measures the peak signal-to-noise ratio to assess overall reconstruction quality, while MSE quantifies the average absolute pixel deviation, providing complementary objective criteria that are more reliable than subjective visual inspection alone.The mean square error (MSE) and peak signal-to-noise ratio (PSNR) after filtering under different salt-and-pepper noise densities are shown in Tables 1 and 2, respectively.

Table 1. Mean square error (MSE) after filtering with different Salt and pepper noises.

	Salt and pepper noise density									
	1.0	1.5	2.0	2.5	3.0	3.5	4.0	4.5	5.0	5.5
median filtering	32.74	32.98	33.25	33.42	33.64	33.99	34.00	34.34	34.57	34.97
adaptive median filtering	9.66	12.59	16.04	20.26	25.38	31.33	38.05	46.19	53.65	63.43
This article improves filtering	13.86	14.22	14.52	15.01	15.37	15.76	16.19	16.36	16.83	17.36

 doi:10.20944/preprints202604.2228.v1

Table 2. Peak signal-to-noise ratio (PSNR) after filtering with different Salt and pepper noises.

	Salt and pepper noise density										
	1.0	1.5	2.0	2.5	3.0	3.5	4.0	4.5	5.0	5.5	mean
median filtering	32.98	32.95	32.91	32.89	32.86	32.82	32.82	32.77	32.74	32.69	32.903
adaptive median filtering	38.28	37.13	36.08	35.06	34.09	33.17	32.33	31.49	30.83	30.11	30.837
This article improves filtering	36.71	36.60	36.51	36.37	36.26	36.16	36.04	36.00	35.87	35.74	36.326

The proposed filter shows competitive performance in terms of PSNR and MSE metrics, and importantly, it preserves edge structures more effectively due to the Laplacian-based edge protection mechanism. As illustrated in Figure 3, adaptive median filtering yields good results at lower salt-and-pepper noise densities. However, at higher noise densities, its performance deteriorates, with some noise points remaining due to the filter's inability to fully remove all noise. In contrast, the edge-adaptive median filtering method proposed in this paper not only achieves a 10.4% improvement in PSNR over traditional median filtering but also prevents excessive filtering, thereby preserving more edge details. Compared to several other filtering methods, the proposed algorithm results in a noticeable improvement in signal-to-noise ratio (SNR). Although the proposed filter does not achieve the highest PSNR among all noise densities, it demonstrates superior edge preservation due to the Laplacian-based edge protection mechanism, which is more critical for subsequent edge detection tasks. The edge-adaptive median filtering effectively reduces noise while maximizing the preservation of image structure, ensuring minimal alteration to the image.

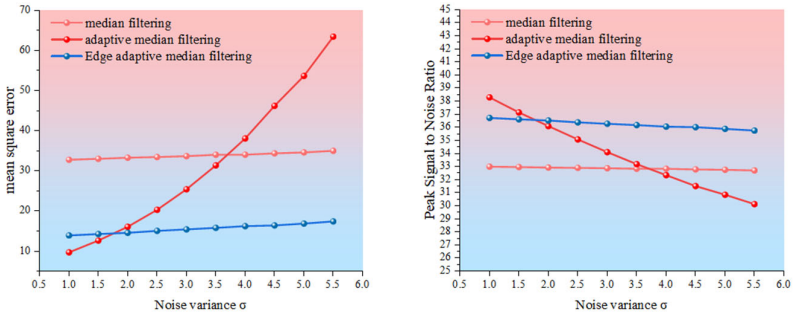

Figure 3. Different Salt and pepper Noise PSNR after filtering.

5.2. Canny Operator Experimental Results

To comprehensively evaluate the edge detection capability of the proposed algorithm, a comparative study was conducted on four representative images: the standard test images 'Lena', 'Cameraman', and 'Peppers', along with a specially collected industrial image 'Invt'. The performance of our proposed method was rigorously compared against three classical edge detection operators: the Canny algorithm, the Laplacian of Gaussian (LOG) operator and Roberts operator . The edge detection results for all four images are visually compared in Figure 4. This qualitative analysis allows for the assessment of key aspects such as edge continuity, noise suppression, and the preservation of structural details across different algorithms and image types.

 doi:10.20944/preprints202604.2228.v1

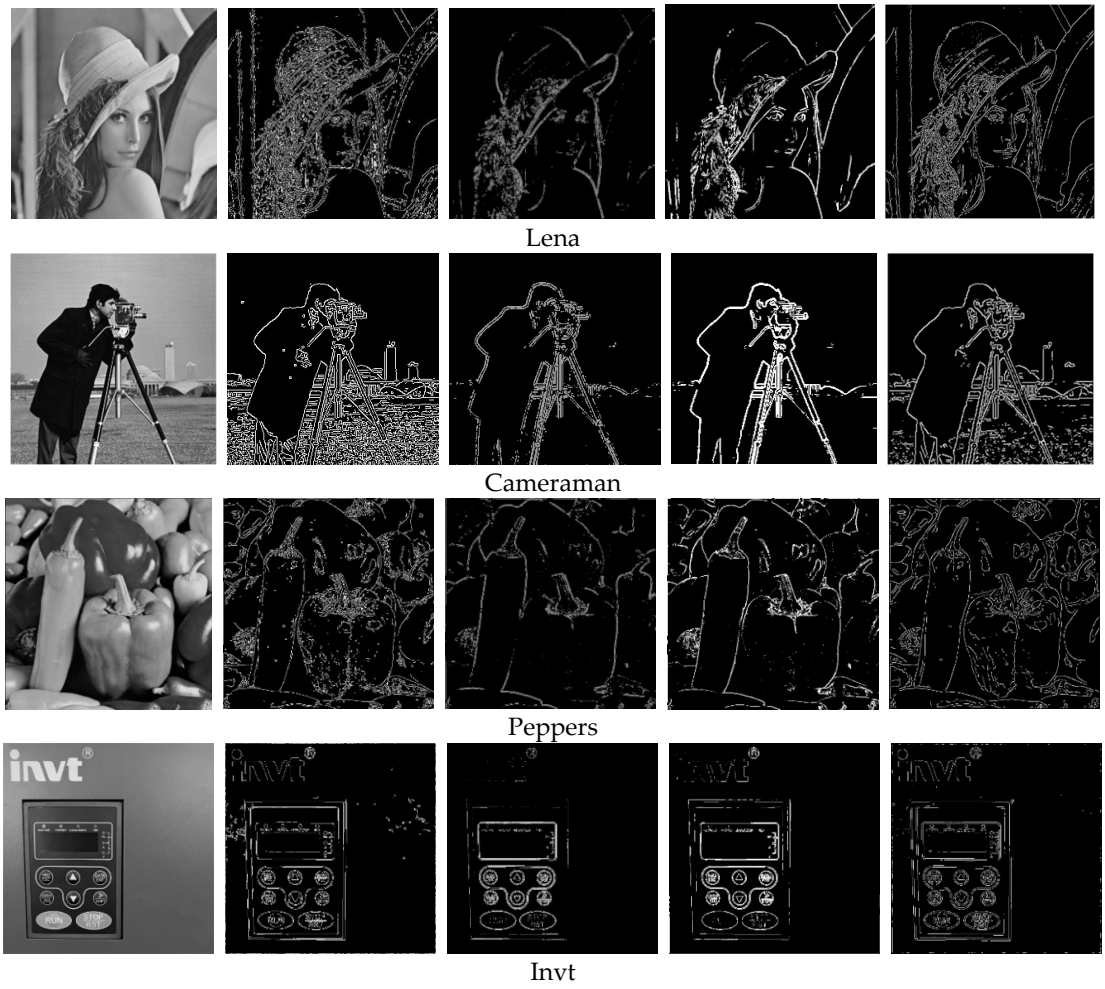

Figure 4. Comparison of Different Algorithm Processing.

According to the comparative analysis in Figure 4, the LOG and Roberts operators are less sensitive to edge lines, resulting in excessive edge loss. When using the Roberts operator for edge detection, the edges in the resulting image may suffer from breakage and thickness due to the influence of noise. In contrast, the traditional Canny operator provides more accurate edge localization, although incomplete edge lines may still occur. The algorithm proposed in this paper demonstrates higher precision in handling edge details compared to the traditional Canny operator, retaining more edge information. This characteristic enables the algorithm to better capture subtle changes in the image's fine structure, improving both edge detection accuracy and the visual quality of the image. Furthermore, the proposed algorithm takes into account noise suppression and edge enhancement factors, effectively balancing edge detection sensitivity and noise resistance, thereby providing a more accurate and reliable foundation for subsequent image processing.The parameters of edge connectivity for several algorithms are shown in Tables 3 and 4.The comparison of edge connectivity parameters is shown in Figure 5.

Based on the objective evaluation method for edge connectivity described in reference [8], the experimental results were statistically analyzed by counting the total number of edge points (A), the number of connected components in the 4-neighborhood (B), and the number of connected components in the 8-neighborhood (C). A smaller value of C/A indicates fewer redundant edge points in the image, fewer discontinuities in the detected edge contours, and higher edge connectivity. A smaller value of C/B indicates better single-edge response.

 doi:10.20944/preprints202604.2228.v1

Table 3. Comparison of parameter C/A for edge connectivity degree.

	Lena	Cameraman	Peppers	Invt
Canny	0.042	0.054	0.050	0.023
LOG	0.137	0.123	0.140	0.101
Roberts	0.060	0.143	0.108	0.130
This paper	0.022	0.015	0.023	0.016

Table 4. Comparison of parameter C/B for edge connectivity degree.

	Lena	Cameraman	Peppers	Invt
Canny	0.194	0.242	0.253	0.141
LOG	0.411	0.302	0.460	0.368
Roberts	0.479	0.509	0.524	0.508
This paper	0.142	0.135	0.142	0.124

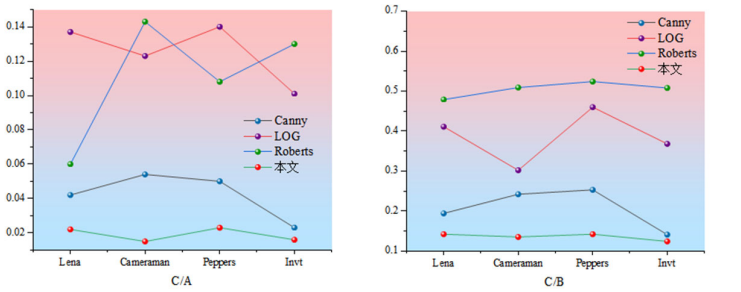

Figure 5. Comparison of parameters for edge connectivity degree.

According to the analysis in table3 and 4, for the images *Lena*, *Cameraman*, *Peppers*, and *Invt*, the values of the proposed modified Canny operators C/A and C/B are both lower than those of the classical Canny operator, LOG operator, and Roberts operator, demonstrating better single-edge response and improved edge image connectivity. Specifically, the C/A value is on average 55.02% lower than that of the classical Canny algorithm, and the C/B value is on average 34.55% lower than that of the classical Canny algorithm. The experimental results indicate that the modified Canny algorithm exhibits higher sensitivity in edge point detection and a significant improvement in maintaining image connectivity. Compared to the traditional Canny operator, the proposed modified Canny operator achieves better edge continuity.

5.3. Zernike Moment Detection Algorithm Experimental Results

In order to conduct a qualitative analysis of traditional and improved algorithms intuitively, a calibrated camera was used for image acquisition, and four different specifications of workpieces were selected for experimental analysis. To ensure a fair comparison, the same pixel-level edge image (extracted by the proposed improved Canny operator described in Section 2) was used as input for both the traditional Zernike moment algorithm and the improved Zernike moment algorithm. Figure 6 shows the edge, radius, and center data of the inspected workpiece, and Table 5 shows the experimental results of the traditional Zernike and the improved Zernike.

 doi:10.20944/preprints202604.2228.v1

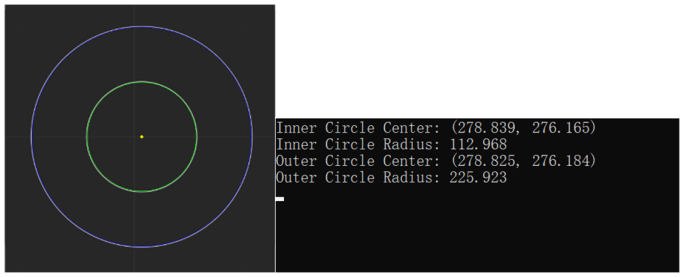

Figure 6. Detected edge, radius, and center data.

Table 5. Comparison of Traditional Zernike and Improved Zernike Experiments.

	Ideal data /mm	Traditional Zernike moment algorithm		relative error %	Improving Zernike moment algorithm		relative error %
		Pixel value /pixel	actual value /mm		Pixel value /pixel	actual value /mm	
Workpiece1							
Inner circle radius	5.0	113.519	5.0289	0.578%	112.968	5.0066	0.132%
Outer circle radius	10.0	226.756	10.0453	0.453%	225.923	10.0147	0.147%
workpiece2							
Inner circle radius	10.0	226.582	10.0376	0.376%	225.935	10.0089	0.089%
Outer circle radius	15.0	340.032	15.0634	0.423%	338.914	15.0139	0.093%
workpiece3							
Inner circle radius	14.0	316.738	14.0315	0.225%	316.194	14.0074	0.053%
Outer circle radius	20.0	452.772	20.0578	0.289%	451.822	20.0157	0.079%
workpiece4							
Inner circle radius	17.0	384.400	17.0289	0.170%	383.874	17.0056	0.033%
Outer circle radius	24.0	542.928	24.0517	0.215%	542.068	24.0136	0.057%

From the comparison of measurement data in Table 5, the improved Zernike moment algorithm demonstrates significant advantages in accuracy over the traditional algorithm. The relative errors of the traditional algorithm range from 0.17% to 0.58%, while the improved algorithm keeps all errors below 0.15%. For some measurements (e.g., the inner radius of Workpiece 1), the error is only 0.132%, representing an improvement of more than one order of magnitude. This indicates that the improved algorithm achieves more accurate sub-pixel edge localization and effectively suppresses the influences of image noise, discretization errors, and edge blurring.

6. Conclusions

This paper presents an enhanced measurement method for circular hole components that effectively addresses precision limitations inherent in industrial visual inspection. The proposed approach integrates an improved Canny operator for robust pixel-level edge detection with an optimized Zernike moments algorithm for high-accuracy subpixel localization. Key innovations include a refined Laplacian-based edge-adaptive denoising technique, multi-directional gradient computation across 16 orientations, and adaptive threshold selection using higher-order moments.

 doi:10.20944/preprints202604.2228.v1

Experimental validation confirms the method's superior accuracy in dimensional measurement of inner and outer diameters through least-squares fitting, demonstrating a significant average error reduction of 75.1% compared to conventional techniques while maintaining computational efficiency suitable for real-time industrial applications.

Author Contributions: Conceptualization, W. Zhang and S. Dong; methodology, W. Zhang; software, W. Zhang; validation, W. Zhang and S. Dong; formal analysis, W. Zhang; writing—original draft preparation, W. Zhang; writing—review and editing, W. Zhang and S. Dong; visualization, W. Zhang; supervision, W. Zhang; project administration, W. Zhang; funding acquisition, S. Dong. All authors have read and agreed to the published version of the manuscript.

Funding: This research was funded by the 2025 Enterprise Horizontal Project "Design of Permanent Magnet Synchronous Motor Controller for Electric Vehicles", grant number 902/22050124092. The APC was funded by the authors.

Institutional Review Board Statement: Not applicable. This study did not involve humans or animals.

Informed Consent Statement: Not applicable.

Data Availability Statement: Not applicable. No new data were created or analyzed in this study.

Acknowledgments: The authors would like to thank their graduate students and colleagues for their valuable discussions and assistance during this research. Special thanks go to the Shanghai-based enterprise for providing the project support that made this work possible.

Conflicts of Interest: The authors declare no conflicts of interest.

References

1. Chen Mingxi, Hou Tao, Zhao Yanzhang, etc Research on Rail Edge Detection Based on New Improved Canny Algorithm [J]. Foreign Electronic Measurement Technology, 2021, 40 (11): 48-52. DOI: 10.19652/j.cnki.femt.2103052.
2. Liu Yuan, Xia Chunlei A Sobel operator based edge detection algorithm for surface defect images of strip steel [J]. Electronic Measurement Technology, 2021, 44 (03): 138-143. DOI: 10.19651/j.cnki. emt. 2005470.
3. Chen Siji, Wang Xiaohong, Li Yunchuan Research on Improving Laplace's UAV Image Edge Detection Algorithm [J]. Surveying Engineering, 2021, 30 (02): 36-44. DOI: 10.19349/j.cnki.issn1006-7949.2021.02.007.
4. Ghosal S，Mehrotra R.Orthogonal moment operators for subpixel edge detection[J].Pattern Recognition，1993，26（2）：295-306.
5. Bin T J，Lei A，Jiwen C，et al.Subpixel edge location based on orthogonal Fourier-Mellin moments[J].Image and Vision Computing，2008，26（4）：563-569.
6. WU Y Q，LONG Y L，ZHOU Y． Sub—pixel edge detection of tool image based on Arimoto entropy and Zernike moment［J］． Journal of South China University of Technology (Natural Science Edition) ，2017，45(12) : 50-56.
7. Thomas S ,Michael M ,Antoine W , et al.Rotation invariant visual processing for spatial memory in insects.[J].Interface focus,2018,8(4):20180010.
8. Qu Guoqing, Li Gan Research on Intelligent Detection Method and System Implementation of Container Sealing [J]. Journal of Electronic Measurement and Instrumentation, 2018, 32 (12): 163-170. DOI: 10.13382/j.jemi.2018.12.022.
9. Chen Xiaowei, Xu Chaohui, Guo Haitao, etc General sub-pixel edge detection method using extreme gradient [J]. Journal of Surveying and Mapping, 2014, 43 (05): 500-507. DOI: 10.13485/j.cnki.11-2089.2014.0073.
10. Singh C ,Bala A .A local Zernike moment-based unbiased nonlocal means fuzzy C-Means algorithm for segmentation of brain magnetic resonance images[J].Expert Systems With Applications,2019,118625-639.
11. Guo J ,Yang Y ,Chen X .Research on sub-pixel accuracy flange disk dimension measurement based on machine vision[J].Signal, Image and Video Processing,2024,18(8-9):6185-6195.
12. Li H, Wang J, Zhang Y. Sub-pixel edge detection based on adaptive Zernike moments and genetic algorithm optimization[J]. Measurement, 2024, 224: 113892.

 doi:10.20944/preprints202604.2228.v1

13. Chen Y, Liu S, Wu Z. Improved Canny edge detection with adaptive median filter for noisy images[J]. Signal Processing, 2023, 205: 108876.
14. Wang Q, Sun L, Zhao X. High-precision measurement of circular holes using machine vision and sub-pixel edge localization[J]. Optics and Lasers in Engineering, 2024, 172: 107865.
15. Zhang R, Li P, Guo F. A novel sub-pixel edge detection method combining deep learning and Zernike moments[J]. IEEE Transactions on Instrumentation and Measurement, 2025, 74: 1-12.
16. Liu Y, Chen W, Zhou T. Edge-preserving adaptive filtering for salt-and-pepper noise removal[J]. Journal of Visual Communication and Image Representation, 2023, 90: 103724.